Formation of Co(II), Ni(II), Zn(II) complexes of alternative metal binding heptapeptides and nitrilotriacetic acid: Discovering new potential affinity tags

Amber Flores, Oladapo Falokun, Ayobami Ilesanmi, Anna Arredondo, Linh Truong, Nayeli Fuentes, Riccardo Spezia, Laurence A Angel

Formation of Co(II), Ni(II), Zn(II) Complexes of Alternative Metal Binding Heptapeptides and Nitrilotriacetic Acid: Discovering New Potential Affinity Tags

Amber Flores,[a] Oladapo Falokun,[a] Ayobami Ilesanmi,[a] Anna Arredondo,[a] Linh Truong,[a] Nayeli Fuentes,[a] Riccardo Spezia,[b] Laurence A. Angel[a*]

[a] *Department of Chemistry, Texas A&M University-Commerce, 2600 S Neal Street, Commerce, TX, 75428, USA* [b] *Laboratoire de Chimie Théorique, Sorbonne Université, UMR 7616 CNRS, 4, Place Jussieu, 75005 Paris, France*

Keywords: His-Cys-Asp peptides; zinc(II)-peptide complexes; nickel(II)-peptide complexes; cysteine metal binding; aspartate metal binding; histidine metal binding; immobilized metal affinity chromatography; peptide tags.

*Corresponding author: Dr. Laurence Angel, Department of Chemistry, Texas A&M University-Commerce, 2600 S Neal St., Commerce, TX, 75428, USA, E-mail: Laurence.Angel@tamuc.edu

Abstract

Using electrospray ionization-ion mobility-mass spectrometry (ESI-IM-MS) a new series of alternative metal binding-5 (amb_5) heptapeptides that provide various combinations of His, Cys and Asp as potential metal binding sites are compared for their relative formation of complexes with the metal ions Co(II), Ni(II) and Zn(II). These amb_5 peptides have the general primary structure acetyl-Aa_1-Aa_2-Gly_3-Pro_4-Tyr_5-Aa_6-Aa_7, where $Aa_{1,2,6,7}$ are the four amino acids that include the His, Cys, and/or Asp potential metal binding sites. The study includes two polyhistidine heptapeptides; the His-tag and His-tag with Pro_4, because they represent the widely applied His affinity tag used in expression cloning and purification of recombinant proteins with immobilized metal affinity chromatography (IMAC). We compare these amb_5 heptapeptides for their formation of the amb_5+M(II) and amb_5+M(II)+NTA complexes, where M = Co, Ni, or Zn, and NTA is nitrilotriacetic acid as a model for the binding of amb_5 in a IMAC column. Overall, the results show that the inclusion of Asp at positions 1, 2, and 7; *i.e.,* ac-Asp_1-Asp_2-Gly_3-Pro_4-Tyr_5-Aa_6-Asp_7, generally favors the formation of amb_5+Ni(II) and amb_5+Ni(II)+NTA complexes, while the inclusion of Cys at positions 2 and 6; *i.e.,* ac-Aa_1-Cys_2-Gly_3-Pro_4-Tyr_5-Aa_6-Cys_7, with Aa_1 = His, Cys or Asp, favors the formation of amb_5+Zn(II) complexes. The comparison with the His-tag and competition between Ni(II) and Zn(II) for forming the amb_5+M(II)+NTA complexes, showed the structure ac-Asp_1-Asp_2-Gly_3-Pro_4-Tyr_5-His_6-Aa_7, with Aa_7 = Cys or Asp, were the most selective for Ni(II) and forming the amb_5+Ni(II)+NTA complex. Collision-induced dissociation of the single negatively-charged $[amb_5+Ni(II)+NTA]^-$ shows it competitively dissociates into $[amb_5-3H+Ni(II)]^-$ or $[NTA-3H+Ni(II)]^-$ while the doubly-charged $[amb_5+Ni(II)+NTA]^{2-}$ complex dissociates into $[NTA-3H+Ni(II)]^-$ and $[amb_{5J}-H]^-$, indicating these complexes are realistic mimics for the complex inside an IMAC column.

1. Introduction

The consecutive series of 5 to 7 His residues added to either the N- or C-terminal of a protein sequence is used in the production and purification of recombinant proteins.[1-3] The vector is introduced into an expression system such as a bacteria and results with the recombinant protein being expressed with a His-tag. These proteins can now be purified because the His-tag will bind to the nickel, cobalt or zinc ions used in immobilized metal ion affinity chromatography (IMAC). The IMAC support resin is usually cross-linked agarose derivatized with nitrilotriacetic acid (NTA) which acts as the chelators for immobilizing the Ni(II), Co(II), or Zn(II) ions inside the column. The His-tagged proteins will bind to these metal sites and be retained inside the column while the non-tagged proteins will wash through. Elution of the His-tagged proteins from the column is achieved with washing the column with a high concentration of imidazole (>200 mM, pH < 5) or a pH 7 to pH 4 gradient. Nickel(II) is most commonly used for IMAC and provides high binding efficiency to His-tagged proteins but also tends to bind to non-target proteins that contain multi-histidines. Cobalt(II) exhibits a higher specific binding of the His-tagged proteins but with a lower loading capacity than nickel(II) and is preferred when high purity is the objective. Zinc(II) binds the His-tagged proteins with a higher loading capacity than cobalt(II) or nickel(II) but with less selectivity, so zinc(II) is used when purity is the least essential. However, the lack of heterogeneity in the His-tag can result in problems of toxicity,[1] stability[4] and aggregation of the recombinant tagged proteins into inclusion bodies in the host cell.[5] Due to these problems, discovering alternative metal binding (amb) peptides with more heterogeneity in their structure could be beneficial for improving solubility, expression, and purification techniques of recombinant proteins.

Previous electrospray - ion mobility - mass spectrometry (ESI-IM-MS) studies of methanobactin[6, 7] from *Methylosinus trichosporium* (mb-OB3b) and the amb peptides whose primary structure replaced the two enethiol oxazolone of mb-OB3b with the 2His-2Cys substituent groups of a zinc finger protein, have shown their potential for applications as affinity tags.[8-15] For example, the ESI-IM-MS analyses of

the amb peptides shows that their formation of metal complexes are dependent on pH which is important for controlling the capture and release of tagged proteins in an IMAC column. A major attribute for ESI-IM-MS analyses is that it allows for the pH-dependent behavior of specific *m/z* conformers to be examined. For example, the negative ion analysis of amb_1, ac-His_1-Cys_2-Gly_3-Pro_4-His_5-Cys_6, from solutions held at pH 7 showed the predominant species is the singly-charged $[amb_1–H]^–$, but from solution > pH 8, the predominant species becomes the complex in the form of the $[amb_1–3H+Zn]^–$.[8, 14] These two species correlate to solution behavior because at pH 7 the observed $[amb_1–H]^–$ relates to the deprotonation of the carboxyl terminus (pK_a ~2.0) and the two His imidazoliums (pK_a ~6.0), while at pH >8, the addition of deprotonation of the two Cys (pK_a~8.3) allows for the chelation of Zn(II) and the formation of the $[amb_1–3H+Zn]^–$ complex. Moreover, the traveling wave ESI-IM-MS measured collision cross section (CCS_{He}) of the $[amb_1–3H+Zn]^–$ complex is consistent with the tetrahedral coordination of Zn(II) via the 2Cys, His_6 and carboxyl terminus, which is also indicative of the metal complex conformation being preserved during the ESI transfer into the gas phase.

From the series of studies of the amb_5 peptides[11, 13, 15] it was originally found that the amb_{5A}, ac-His_1-Cys_2-Gly_3-Pro_4-Tyr_5-His_6-Cys_7 (Fig 1),[11] also exhibited a single negatively-charged complex that co-ordinated the Zn(II) via a distorted tetrahedral geometry which density functional theory (DFT)[11] indicated were either the substituent groups of His_1-Cys_2-His_6-Cys_7 or the thiolate of Cys_2, backbone carbonyl O of Cys_2, thiolate of Cys_7 and the carboxylate terminal. These DFT structures which contained *cis*-Pro had theoretical CCS_{He} that were 20 Å^2 to 31 Å^2 larger than those measured by the ESI-IM-MS analyses. In further ESI-IM-MS and DFT studies of a series of amb_5 peptides with modifications to the 2Cys, 2His and carboxyl terminus sites[13] (Fig 1, amb_{5A-G}), indicated that the imidazoles acted as proton acceptors for the deprotonation of the thiol groups which became the anchoring sites for Zn(II) at pH 7. A new Zn(II) *trans*-Pro complex was also discovered that although higher in free energy than the *cis*-Pro conformers, exhibited a DFT CCS_{He} in good agreement with the ESI-IM-MS measured CCS_{He} with Zn(II) coordinated via the substituent groups of the His_1-Cys_2-Cys_7 and the carboxylate terminus.[13, 15]

Further studies of the Zn(II) and Ni(II) chelation by a similar series of modified amb_{1A-H} peptides,[14] and comparison with the amb_{5A-F} peptides showed that the additional Tyr in the amb_5 structures contributed to their greater selectivity for Zn(II) at pH 7.0. Why the amb_5 peptides had a preference for chelating Zn(II) over Ni(II) at pH 7.0 is further studied here by extending the amb_5 series to include twelve new primary structures to determine whether differences in their primary structure will influence their formation of Zn(II), Ni(II) or Co(II) complexes. The new amb_5 heptapeptides **G** to **R**, have the general primary structure acetyl-Aa_1-Aa_2-Gly_3-Pro_4-Tyr_5-Aa_6-Aa_7, where the two amino acid on each of the terminals are the potential metal binding sites and include the side groups of His, Cys, and/or Asp residues (Fig 1). The three central amino acids are Gly_3 a spacer, Pro_4 the hinge for the N- and C-terminal arms, and Tyr_5 providing a π-metal cation interaction and hydrogen bond to the C-terminus. For comparison with amb_{5A} the new structures **G** to **R** replace His_1 with either Cys_1 or Asp_1, Cys_2 with either Asp_2 or His_2, Tyr_5 with either Phe_5 or Gly_5, His_6 with Cys_6, and Cys_7 with either Asp_7 or His_7. The study also includes the 7xHis-tag, **P**, and the 6xHis-tag with Pro_4, **O**, so a comparison can be made to the established His-tag. Here we compare the total Zn(II), Ni(II) or Co(II) binding of amb_{5A-R}, measured from both positive and negative ion analyses from solutions at pH 7 and look into more detail into the negatively-charged Ni(II) and Zn(II) complexes formed by the new amb_5 **G** to **R**. The formation of the amb_5+M(II)+NTA complex, where M = Ni or Zn and NTA = nitrilotriacetic acid, which mimic the formation of complexes in an IMAC column are also studied to give insight into which amb_5 peptides may be potentially useful as alternatives to the His-tags for the purification of recombinant proteins.

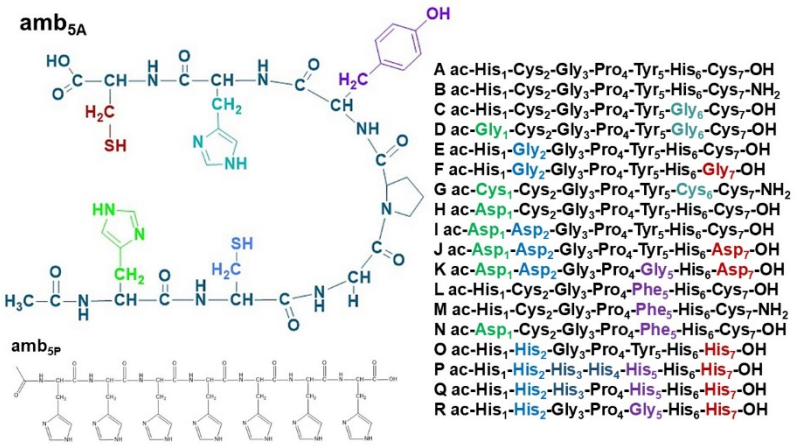

Figure 1. The primary structure of alternative metal binding-5A (amb_{5A}) with the color highlighting the regions modified with respect to the listed primary structures of amb_5 peptides **A** to **R**. The structure of amb_{5P} is also shown, which is the 7xHis-tag.

2. Experimental section

2.1 Reagents, stock and working solutions

The alternative metal binding-5 (amb_5) peptides **A** to **R** were synthesized by PepmicCo (http://www.pepmic.com/). Stock and working solutions were prepared with deionized (DI) water >17.5 MΩ cm (http://www.millipore.com). Ammonium acetate (ultrapure) was purchased from VWR (https://us.vwr.com/). Ammonium hydroxide (trace metal grade) was purchased from Fisher Scientific (http://www.Fishersci.com/). Zinc nitrate hexahydrate (99%+ purity) was purchased from Alfa Aesar (www.alfa.com/), cobalt(II) acetate (99.99%) was purchased from Sigma-Aldrich (www.sigmaal-drich.com/), and nickel(II) nitrate hexahydrate (99% purity) was purchased from ACROS (https://www.acros.com/).

2.2 Sample preparation and ion mobility – mass spectrometry analysis

The ammonium acetate (10.0 mM) was pH adjusted with ammonium hydroxide to create a pH 7.4 solution. Each individual sample was prepared with one of the amb_5 peptides, pH adjusted with the ammonium acetate/ammonium hydroxide (AA/H) solution, before an equimolar amount of the metal ion was added. The final solutions for ESI-IM-MS analysis contained both the amb_5 and metal ion at 12.5 µM

with the AA/H at 8.0 mM. For the amb_5+metal+NTA samples they were prepared in the same order, but included the NTA after the addition of the metal ion. For these samples the final concentration of amb_5 and metal was 12.5 μM each, NTA 25.0 μM and 8.0 mM buffer solution. The samples for studying the competitive binding of Ni(II) or Zn(II) metals were made at final concentrations of the NTA: amb_5: Ni(II): Zn(II) of 25 μM:12.5 μM:6.25 μM:6.25 μM respectively in AA/H solution at pH 7.4. All solutions were mixed aerobically at room temperature and left to stand for 10 minutes. Half of the sample was used for ESI-IM-MS analysis and the other half to measure the final pH of the sample, using a calibrated Orion 98 micro pH electrode. The final pH of the solutions were between pH 6.9-7.2. The samples were electrosprayed into the Waters Synapt High-Definition Mass Spectrometer (G1)[16] with ESI conditions and traveling wave settings optimized to limit any structural rearrangement or dissociation of the amb_5 species. Typical operating conditions are described in the Supporting Information.

2.3 Analysis of the metal+amb_5 data

The ESI-IM-MS analysis allowed for *m/z* identification and drift time separation of all the species in the amb_5+metal and amb_5+metal+NTA samples. The positively- and negatively-charged species were identified based on their *m/z* isotope patterns with the detector kept at a minimal voltage of 1650 V to exclude ripple of the baseline between arriving isotopes of the most intense species. The arrival time distributions (ATDs) of amb_5 ions were determined by the time they spent traveling through the ion mobility cell and measured by their *m/z* arrival time response at the detector of the time-of-flight mass analyzer. The different mass-to-charge species and their ATDs were extracted using the Driftscope 2.0 software. The areas under the ATD curves were integrated using the MassLynx 4.1 software and used to determine the relative intensity of each species by normalizing their area to the sum of the areas of all identified amb_5 species in each analyzed sample. For the bar graphs that show contributions from both negative and positive ions, each contribution was halved to normalize back to a percentage scale. Each experiment were repeated three to five times to calculate the mean and the standard deviations.

2.4 Computational Methods

To locate geometry optimized conformers of the amb_5 metal complexes, we used density functional theory (DFT) and in particular the popular B3LYP functional[17, 18] and M062X[19, 20] using two basis sets: LanL2DZ and Def2SV. All DFT calculations were done with Gaussian 09 software.[21] The starting structures for the geometry optimizations of the Zn(II) and Ni(II) complexes where based on our previously located B3LYP conformers,[13, 15] where all peptide bonds are in their *trans* configuration, including the *trans*-Pro_4, and the metal ligating sites are the side groups of the residues in the Aa_1-Aa_2-Aa_7 positions and include the carboxylate terminus in a distorted tetrahedral coordination geometry, *i.e.* singlet spin state for Zn(II) and triplet spin for Ni(II). The free energy difference for the reaction $[amb_5\text{-}3H+Zn(II)]^- + Ni(II) \leftrightarrow [amb_5\text{-}3H+Ni(II)]^- + Zn(II)$ were calculated, with single point energies also calculated from the geometry-optimized LanL2DZ and Def2SV conformers using the 6–31++g(d,p) basis set for C, N, O, S and H atoms with the (14s9p5d) primitive set of Wachters[22] supplemented with one s diffuse function, two p diffuse functions, one d diffuse function and one f polarization function, are used for the metal ions so that the final contracted basis set was [10s7p4d1f]. Note that the diffuse functions were included because of their well-known importance for correctly describing the anionic systems modelled here. This more extended basis set, defined from now on as "mix", was previously successfully used to study the structure and reactivity of amino-acids binding open shell Co(II).[23, 24] The CCS_{He} of each located B3LYP conformer was calculated using the ion size scaled Lennard-Jones (L-J) method,[25] provided by the Department of Chemistry and Biochemistry, UCSB, from ten measurements to determine the mean and standard deviation of the L-J CCS_{He} and compare with the ESI-IM-MS measured CCS_{He}.

3. Results and Discussion

3.1 Comparative selected metal chelation by $amb_{5A\text{-}R}$ at pH 7.0

To compare the relative formation of Co(II), Ni(II) and Zn(II) complexes by amb_5 **A** to **R**, Fig 2 shows the average percent of positive and negative ion complexes formed from the equimolar metal:amb_5 solutions at pH 7.0. The results are the sum of the different metal complexes formed and include the amb_5 species binding one or two metal ions and in some cases amb_5 dimers binding metals, as a percentage of

all the identified bound and free amb$_5$ species from each trial. Figure 2 also includes some previously published results[13, 15] for the formation of Ni(II) and Zn(II) complexes by **A** to **F** for comparison.

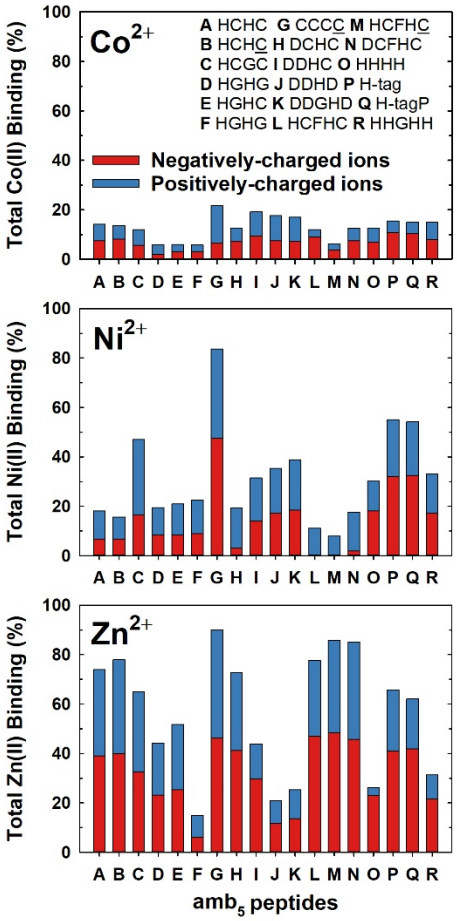

Figure 2. Comparison of the total binding of Co(II), Ni(II) or Zn(II) by the amb$_5$ peptides **A** to **R** measured from the averaged positive and negative ion analyses of the 12.5:12.5 μM mixture of metal(II):amb$_5$. The results are the means from 3-5 separate trials from solutions at pH 7.0, with standard deviations between 1 to 5% for Ni(II) and 1 to 9% for Zn(II) and Co(II). The names of the amb$_5$ have been abbreviated to their one letter amino acid sequence in the Aa_1-Aa_2-Aa_6-Aa_7 positions with the Aa_7 residue underlined if amidated and the Aa_5 residue included if it has been changed from Tyr (Y).

3.2 Comparative Co(II) chelation by amb$_{5A\text{-}R}$ at pH 7.0

The results in Fig 2 show the formation of Co(II) complexes were the lowest for the three metals, with the formation of Co(II) complexes < 22% for all the amb$_5$. The species **G**, **I**, **J**, and **K** have the slightly higher apparent total binding of Co(II) and their sequences contain predominantly Cys or Asp as binding groups. The amb$_5$ **G** formed complexes of the dimer binding 2Co(II), *e.g.,* [diamb$_{5Gox}$+2Co(II)] and [diamb$_{5Gdiox}$+2Co(II)], where diamb$_{5Gox}$ is the dimer held together by an intermolecular disulfide bond

(*ox*), and diamb$_{5G}$di*ox* has two intermolecular disulfide bonds (di*ox*), respectively. These species were observed in the positive and negative ion analyses as 2+ or 2– charged complexes. However, the species of **I**, **J**, and **K**, which contained 2-3 Asp, primarily bound a single Co(II) as the 2+ or 2– charged [amb$_5$+Co(II)] complexes. The [amb$_5$+Co(II)]$^{2\pm}$ complex was also the primary contributor to the poly-His peptides **O**, **P**, **Q** and **R**, indicating the binding of Co(II) was via the imidazoles for positive ions and via the imidazolates for negative ions. The amb$_5$ species with 2His-2Cys, His-2Cys or Asp-His-2Cys sites formed < 14% Co(II) complexes and had the highest relative uncertainties 5-9%.

3.3 Comparative Ni(II) chelation by amb$_{5A\text{-}R}$ at pH 7.0

The comparative formation of Ni(II) complexes by the amb$_5$ species **A** to **R** (Fig 2) showed that **G** (85%) exhibited the highest followed by **P** (55%), **Q** (54%), and **C** (47%). Our previous ESI-IM-MS amb analyses, have shown that the negatively-charged complexes are of particular interest because they correlate to the charge states that relate to the protonation state of the Cys, His, or carboxyl termini which are the potential metal ligand sites and they exhibit a distinct pH-dependence.[8-15] In Figure 3 we show the identity and the relative percentage of these negatively charged complexes for amb$_5$ **G** to **R**. Only **G** primarily formed the [amb$_5$-6H+2Ni(II)]$^{2-}$ complex that related to six negatively-charged sites on the amb$_{5G}$ peptide. Species **G**, as in the Co(II) analyses, also formed the negatively charged dimer binding 2Ni(II), [diamb$_{5ox}$-6H+2Ni(II)]$^{2-}$, where the 2Cys oxidized to form a disulfide bond. Whether the [amb$_5$-6H+2Ni(II)]$^{2-}$ complex is an artifact of the ESI or exists in solution depends on the deprotonation of 4Cys and other sites such as the Tyr or amide groups from the C-terminal or backbone. These sites would also provide the binding sites for the 2Ni(II). Three other species **K**, **P**, and **Q** also formed [amb$_5$-6H+2Ni(II)]$^{2-}$ but ≤ 16% because they primarily formed the [amb$_5$-4H+Ni(II)]$^{2-}$complex instead. Nickel(II) is known to be able to anchor to a side group and bind to deprotonated amide groups in square planar geometry as does Cu(II),[26] although this type of binding requires a low spin state for Ni(II).

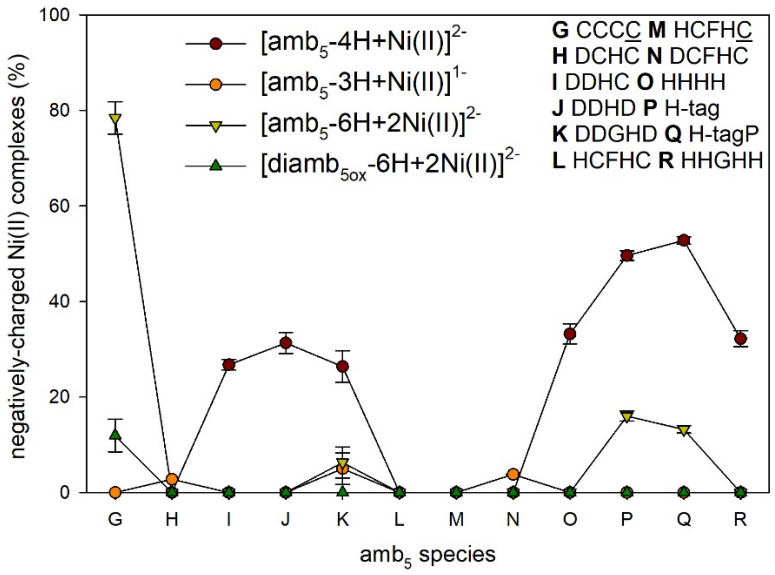

Figure 3. The comparison of the percentage of formation of negatively-charged nickel(II) complexes of amb_5 **G** to **R** measured from 3 separate measurements from solutions at pH 7.0. The error bars are the standard deviations. The names of the amb_5 have been abbreviated to their one letter amino acid sequence in the Aa_1-Aa_2-Aa_6-Aa_7 positions with the Aa_7 residue underlined if amidated and the Aa_5 residue included if it has been changed from Tyr (Y).

The next group that exhibited significant Ni(II) binding were **I**, **J**, **K**, **O**, and **R** which all formed between 30-40% Ni(II) complexes. These negative ion complexes were mainly of the form $[amb_5\text{-}4H+Ni(II)]^{2-}$, with **K** also forming $[amb_5\text{-}3H+Ni(II)]^{-}$ (Fig 3). The species **I**, **J**, and **K** have primary structures described by ac-Asp_1-Asp_2-Gly_3-Pro_4-Aa_5-His_6-Aa_7, where Aa_5 = Tyr or Gly and Aa_7 = Asp or Cys. These $[amb_5\text{-}4H+Ni(II)]^{2-}$ complexes of **I**, **J**, and **K** are consistent with the chelation of Ni(II) by the deprotonated side groups of Asp_1, Asp_2, Aa_7, and the carboxyl terminus, which are the equivalent positioned sites predicted by our previous ESI-IM-MS and DFT studies of **A**, **B**, and **C**.[14, 15] The **H** and **N** species, that are related to **I** but have Cys_2 rather than Asp_2, did not form $[amb_5\text{-}4H+Ni(II)]^{2-}$ and only formed 5% of $[amb_5\text{-}3H+Ni(II)]^{-}$, which indicates that at pH 7.0 the Cys_2 is not an effective binding site for Ni(II) and it remains primarily protonated. For species **H** and **N**, the Cys_7 resides by His_6 a base that could decrease its effective p*K*a, while Cys_2 resides by an acidic group Asp_1 that could increase its effective p*K*a. The species **O** and **R** which have the 4His in their primary structures, ac-His_1-His_2-Gly_3-Pro_4-Aa_5-His_6-His_7, formed only the $[amb_5\text{-}4H+Ni(II)]^{2-}$ complex which is indicative that imidazolates are binding the Ni(II) and contribute to the overall charge. As positive ions **O** and **R** formed

$[amb_5+Ni(II)]^{2+}$ consistent with imidazoles binding Ni(II). For **L** and **M** which contained the 2Cys-2His motif, there was no formation of the negatively-charged Ni(II) complexes indicating their formation was limited by the 2Cys. Therefore, the analyses of the new amb_5 species showed that the most effective chelators of Ni(II), with the exception of **G**, were species that contained multiple Asp (**I**, **J**, **K**) or His (**O**, **P**, **Q**, **R**) side groups.

3.4 Comparative Zn(II) chelation by amb_{5A-R} at pH 7.0

The comparison of amb_5 **A** to **R** in Fig 2 showed **A**, **B**, **G**, **H**, **L**, **M**, and **N** exhibited the highest ≥ 72% formation of Zn(II) complexes. These species have a primary structure described by ac-Aa_1-Cys_2-Gly_3-Pro_4-Aa_5-Aa_6-Cys_7, where Aa_1 = His, Cys or Asp, Aa_5 = Tyr or Phe and Aa_6 = His or Cys. These sequences conserve the positions of Cys_2 and Cys_7 and stipulate that these are the principal Zn(II) binding sites.[13] Species **G** with 4Cys exhibited 90% formation of Zn(II) complexes, the highest of all the amb_5 species. The comparison of **A** with **H** shows that His_1 can be replaced by Asp_1 and still result with 73% formation of Zn(II) complexes. The comparison of **A**, **B**, **H** with **L**, **M**, **N** also indicates the replacement of Tyr_5 with Phe_5 results with small increases in Zn(II) binding to 78-86%.

The comparison of the identity of the negatively-charged Zn(II) complexes formed by the new amb_5 **G** to **R** species are shown in Fig 4. The doubly-charged $[amb_5\text{-}4H+Zn(II)]^{2-}$ is the main complex for all twelve species and shows there are four deprotonated negatively charged sites, which could qualify for the four Zn(II) ligand sites. For **G** these could be the 4Cys thiolate sites and for **H**, **I**, **J**, **K**, and **N** the Asp or Cys at positions Aa_1-Aa_2-Aa_7 with the carboxylate terminus. For **L** and **M** these sites could include the 2Cys thiolates, His imidazolate, and the carboxylate terminus, while for **O**, **P**, **Q**, and **R** the 3His imidazolates and the carboxylate terminus. Species **G** with 4Cys formed 43% of the singly-charged $[amb_5\text{-}3H+Zn(II)]^{-}$, which is more than any of the other amb_5 species, whereas, **O**, **P**, **Q**, and **R**, which have 4-7His, did not form the singly-charged complex but formed the doubly-charged $[amb_5\text{-}4H+Zn(II)]^{2-}$ complex.

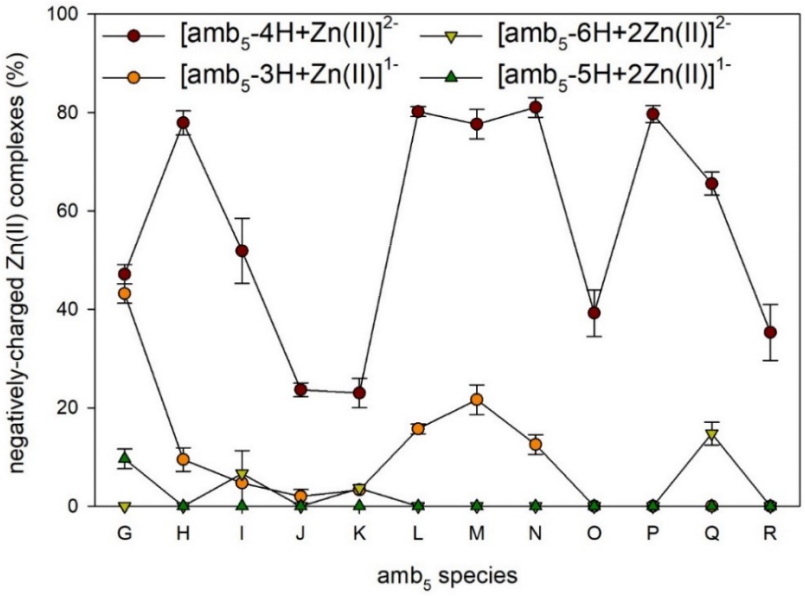

Figure 4. The comparison of the percentage of formation of negatively-charged zinc(II) complexes of amb_5 **G** to **R** measured from 3 separate measurements from solutions at pH 7.0. The standard deviations are used as the error bars.

The His-tag analogs of **P** and **Q** formed the next highest Zn(II) complexes after **G**, **H**, **L**, **M**, and **N**. Species **I** exhibited an intermediate level for forming Zn(II) complexes and contained the thiolate and carboxylate of Cys_7 to coordinate the Zn(II), but had Cys_2 replaced with Asp_2 which showed the formation of Zn(II) complexes was lessened by the absence of the Cys_2 thiolate group. The remaining species **J**, **K**, **O**, and **R**, resulted in the lowest formation of Zn(II) complexes and these did not contain either the Cys_2 or Cys_7 sites in their primary structures, typifying the importance of the two thiolates for chelating Zn(II).

3.5 Density functional theory modeling of amb_5 Ni(II) and Zn(II) complexes and comparison of collision cross sections

Our previous studies[13] have shown that the comparison between DFT theory and ESI-IM-MS experiment were the most conclusive for the single negatively charged species. Here we have located the B3LYP and M06-2X geometry-optimized conformers, using the LanL2DZ and Def2SV basis sets, for selected negatively charged Zn(II) and Ni(II) complexes. The starting structures of these complexes were based on our previously located lowest B3LYP free energy conformers for **A**, **B**, and **C**[13, 15] where the

peptide bonds are in their *trans* configuration, including *trans*-Pro, and the metal ligating sites are the side groups in the Aa_1-Aa_2-Aa_7 positions and the carboxylate terminus. From these conformers the L-J CCS_{He} were calculated and are compared to the ESI-IM-MS measured CCS_{He} for the same species (Table 1). Generally, Table 1 shows there is close agreement between the L-J and ESI-IM-MS CCS_{He} values, with Def2SV giving better agreement than LanL2DZ, with only the **L**-Zn(II) and **K**-Ni(II) complexes exhibiting CCS_{He} outside of their mutual associated uncertainties. Results obtained with M062X functional are less in agreement with respect to experimental collision cross section values and they are listed in Table S1 of the Supporting Information. In the following we discuss B3LYP L-J CCS_{He} results.

Table 1. Comparison of collision cross sections ($Å^2$) from B3LYP theory and experiments.

amb_5	$[amb_5\text{-}3H+Zn(II)]^-$			$[amb_5\text{-}3H+Ni(II)]^-$		
	LanL2DZ	Def2SV	Exp.[a]	LanL2DZ	Def2SV	Exp.[a]
A	202±3	202±3	200	205±4	201±2	199
B	205±3	202±2	203	204±2	202±3	204
C	192±2	193±3	188	192±4	189±4	187
D	174±2	169±1	170	172±1	169±2	172
E	193±2	189±1	194	193±2	192±2	191
F	188±3	186±4	180	186±3	184±2	187
G	189±3	187±2	186	187±3	187±2	-
H	197±2	189±3	189	195±3	188±3	193
I	198±3	193±2	190	197±3	193±2,199±2[b]	191[b]
J	199±2	191±2	194	198±2	189±1,194±2[b]	194[b]
K	188±3	184±3	181	188±4	188±3,190±4[b]	176,183[b]
L	210±3	208±2	192	208±2	207±3	-
M	202±3	200±3	198	202±2	199±3	-
N	199±3	196±2	190	199±2	197±2	193

[a] The ESI-IM-MS CCS_{He} have error bars of ±4 $Å^2$. [b] CCS_{He} for the doubly-charged $[amb_5\text{-}4H+Ni(II)]^{2-}$ complex.

The favorable agreement of the CCS_{He} also suggests that the *m/z* of the amb_5 species are primarily influenced by the protonation state of their acidic and basic sites. For example, the amb_5 species with the carboxyl terminus will favorably form negative ions in solution at pH 7.0, and our previous ESI-IM-MS studies[8, 11, 13-15] have shown that the formation of Zn(II) or Ni(II) complexes are dependent on the pH of the solution ≥ pH 7.0, which relates to the pK_as of the His and Cys binding sites. In Figure 3 it is shown that **I**, **J**, and **K** formed the $[amb_5\text{-}4H+Ni(II)]^{2-}$ complex, whereas, **H** and **N** formed only the $[amb_5$-

3H+Ni(II)]$^{-}$ complex. The comparison of these B3LYP geometry-optimized conformers for **H**, **I**, and **J** are shown in Figure 5, where they all exhibit the distorted tetrahedral coordination of Ni(II) via the Asp_1-Aa_2-Aa_7 and carboxylate terminus. The Cys_7 or Asp_7 sites are of particular importance because their side group and carboxylate terminus concomitantly coordinates the Ni(II) ion. Therefore, the conformer of the singly-charged complex of **H** (Fig 5a) is similar to the conformers of the doubly-charged complexes of **I** and **J** (Fig 5b, c). In all three conformers it is the Asp_1-Aa_2-Aa_7 and C-terminus sites that are deprotonated and it is whether the His_6 δN is protonated on the imidazole ring that changes the overall charge of the complex. For the conformer of **H** the His_6 forms a hydrogen bond to the backbone carbonyl oxygen of Cys_2, which is also present in the conformer of **I** when the His_6 δN is deprotonated. For **J** the His_6 retains its general position by forming a π-cation interaction with Ni(II). For all three complexes in Fig 5 the Tyr_5 phenyl ring also forms a long range π-cation interaction with Ni(II).

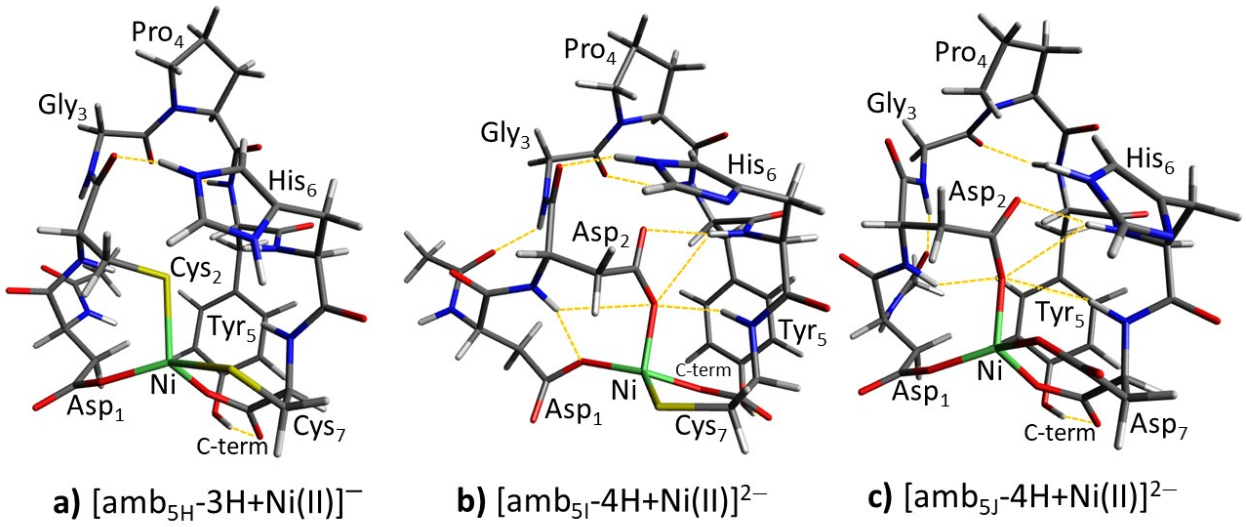

Figure 5. The B3LYP/Def2SV geometry-optimized conformers of a) [amb_{5H}-3H+Ni(II)]$^{-}$ exhibiting Asp_1-Cys_2-Cys_7 and carboxylate terminus coordination of Ni(II), b) [amb_{5I}-4H+Ni(II)]$^{2-}$ exhibiting Asp_1-Asp_2-Cys_7 and carboxylate terminus coordination of Ni(II), and c) [amb_{5J}-4H+Ni(II)]$^{2-}$ exhibiting Asp_1-Asp_2-Asp_7 and carboxylate terminus coordination of Ni(II). Yellow dashed lines indicate hydrogen bonds.

Considering the change in charge for Ni(II) complexes of **H** to **I** and **J** (Figs 3 and 5), it is the replacement of Cys_2 with Asp_2 that changes this charge from a singly- to doubly-charged complex. Our earlier work of amb_{5A},[13] indicated at pH 7.0 a proton transfer from Cys to His resulted in a salt-bridge

between Cys and His in its tertiary structure. The results here also indicate that a proton transfer from Cys_2 to His_6 is resulting in the singly-charged Ni(II) complex of **H**. However, species **H** exhibits relatively low formation of the Ni(II) complex (5%) and it is the replacement of Cys_2 with Asp_2 that results in the increased formation of the Ni(II) complexes by **I**, **J** and **K**. Table 2 shows the comparison of the bond lengths between the ligand sites and Ni(II) in the **H**, **I**, **J** and **K** complexes, indicating the tightest Ni(II) coordination is by species **J** and **K** when each ligand is the oxygen of a carboxylate site. The bond lengths of three common hydrogen bonds; between His_6 and carbonyl oxygens (His_6 H-bond), Gly_3 carbonyl and Tyr_5 amine (Hinge H-bond), and Tyr_5 hydroxyl and the carboxylate terminus (Tyr_5 H-bond) are also shown.

Table 2. Coordination bond lengths and hydrogen bond lengths (Å) for the B3LYP/Def2SV conformers of selected amb_5 Ni(II) complexes.

Bonds	$[amb_{5H}\text{-}3H+Ni(II)]^{-}$	$[amb_{5I}\text{-}4H+Ni(II)]^{2-}$	$[amb_{5J}\text{-}4H+Ni(II)]^{2-}$	$[amb_{5K}\text{-}4H+Ni(II)]^{2-}$
Aa_1–Ni(II)	1.942	2.013	1.942	1.918
Aa_2–Ni(II)	2.387	1.993	2.006	1.999
Aa_7–Ni(II)	2.351	2.273	1.913	1.994
C-term–Ni(II)	1.978	1.958	1.942	1.937
His_6 H–bond	1.918	2.030	-	1.420
Hinge H–bond	2.139	2.046	2.017	1.947
Tyr_5 H–bond	1.660	1.659	1.657	-

Using the B3LYP functional for computing the free energy differences for the reaction $[amb_5\text{-}3H+Zn(II)]^{-} + Ni(II) \leftrightarrow [amb_5\text{-}3H+Ni(II)]^{-} + Zn(II)$ (Table S2) both the LanL2DZ and Def2SV basis sets predicted that the Ni(II) complexes were more favorable in free energy than the Zn(II) complexes. The basis set effect for the differences in free energies were large (see Table S2) and to improve the correlation, a hybrid basis set[22] abbreviated as "mix" was used to calculate single point energies for the LanL2DZ and Def2SV optimized structures, shown in Table 3.[23, 24] However, again the B3LYP method predicts that Ni(II) complexes are more favorable in free energy than the Zn(II) complexes in contradiction to the general ESI-IM-MS results. The comparison of the LanL2DZ//mix and Def2SV//mix results shows that only **E**, **J**, **K**, **L**, and **N** are within 2.5 kJ/mol of one another. For **J** and **K**, which have 3Asp in their structure, there is qualitative agreement with experiment that these two species are more favorably

chelated by Ni(II) over Zn(II) (Figs 2, 3, and 4). However, the ESI-IM-MS results show **L** and **N**, like all the species with 2Cys in their primary structure, exhibit a preference for Zn(II) complex formation (Figs 2, 4) and do not agree with the free energies predicted by the B3LYP with the LanL2DZ//mix and Def2SV//mix basis sets (Table 3). To further investigate the DFT prediction of the free energies differences for the reaction $[amb_5\text{-}3H+Zn(II)]^- + Ni(II) \leftrightarrow [amb_5\text{-}3H+Ni(II)]^- + Zn(II)$, the M062X functional was used with the Def2SV//mix basis set, resulting in a better correlation with the ESI-IM-MS results concerning energetics. In fact, the M062X method predicts that the species with 2Cys prefer Zn(II) over Ni(II) and the species **E** and **F**, where the 2Cys substituent groups are removed, show preference for Ni(II) complexation. For all the other species, M062X calculations suggest that Zn(II) complexes are more stable, even if the difference is relatively small for **I** and **K** species (2.0 and 11.2 kJ/mol, respectively), where the Cys are replaced with Asp. We should note that all the calculations are done in the gas phase, to mimic ESI-IM-MS conditions, but the abundance observed experimentally can be due to the liquid phase which precedes the electrospray. Overall, M062X results support the picture by which Ni(II) chelation is enhanced by removing (or replacing) Cys residues, otherwise Zn(II) species are more favorable.

Table 3. Free energy difference (kJ/mol) for the reaction $[amb_5\text{-}3H+Zn(II)]^- + Ni(II) \leftrightarrow [amb_5\text{-}3H+Ni(II)]^- + Zn(II)$.

	B3LYP		M062X
amb_5	LanL2DZ//mix	Def2SV//mix	Def2SV//mix
A	-28.34	-15.16	43.4
B	-31.19	-17.32	41.7
C	-28.62	-20.93	15.4
D	0.82	-12.93	27.4
E	-30.88	-31.21	-3.8
F	-19.77	-16.47	-31.9
G	-25.34	-23.55	17.6
H	-31.42	-23.99	17.9
I	-27.37	-21.42	2.0
J	-27.37	-25.73	19.8 [a]
K	-19.10	-20.96	11.2
L	-21.04	-23.17	17.4
M	-26.31	-12.54	33.6 [a]
N	-29.40	-27.22	68.6 [b]

[a] Thermal correction for Ni(II) complex at M062X/LanL2DZ level of theory. [b] Optimization and thermal correction for Ni(II) complex at M062X/LanL2DZ level of theory.

3.6 Formation of amb$_5$+metal(II)+NTA complexes at pH 7.0

Thirteen of the amb$_5$ species that showed the highest formation of Ni(II) or Zn(II) complexes were chosen to investigate further their formation of the amb$_5$+metal(II)+NTA complex, where NTA= nitrilotriacetic acid, which mimics the complex inside an IMAC column. Figure 6a shows the percent formation of **C**, **G**, **H**, **I**, **J**, and **N** for the amb$_5$+Ni(II)+NTA complexes were significantly higher than their formation of the equivalent Zn(II) or Co(II) complexes. Of this group, **I** and **J** showed the highest formation of the amb$_5$+Ni(II)+NTA complexes, which coincided with their primary structures having Asp$_1$, Asp$_2$ and Cys$_7$/Asp$_7$. Comparing with **K**, which exhibited a significantly lower formation and selectivity of the Ni(II) complex than **J**, indicated that Tyr$_5$, with the π-cation interaction or hydrogen bonding (Fig 5c), increased the formation of the **J** complex. Species **H** and **N** which contained Asp$_1$ and only differed by the replacement of Tyr$_5$ with Phe$_5$, exhibited a similar selectivity and formation of the Ni(II) complexes.

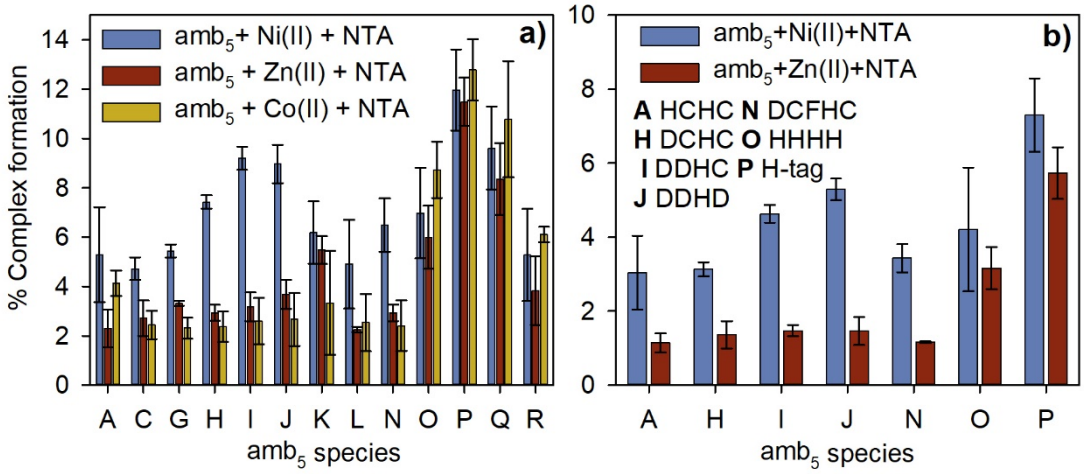

Figure 6. a) Percent formation of the amb$_5$+Ni(II)+NTA (blue), amb$_5$+Zn(II)+NTA (brown), and amb$_5$+Co(II)+NTA (yellow) complexes observed from the averaged negative and positive ion analyses of the 12.5:12.5:25.0 µM mixture of amb$_5$:metal(II):NTA at pH 7.0. **b)** The competition of selected amb$_5$ peptides for forming the amb$_5$+Ni(II)+NTA or amb$_5$+Zn(II)+NTA complexes from12.5:6.25:6.25:25.0 µM mixture of amb$_5$:Ni(II):Zn(II):NTA at pH 7.0. The name of the amb$_5$ have been abbreviated to their Aa$_1$-Aa$_2$-Aa$_6$-Aa$_7$ positions and the Aa$_5$ residue included if it has been changed from Tyr (Y).

The His-tag **P** exhibited the highest formation of all three metal complexes, followed by **Q** and **O**. The interaction between the Ni(II) and NTA is usually depicted via the four sites of the tertiary amine and

three carboxylate groups, leaving two sites for the His-tag to complete an octahedral coordination.[2] However, the His-tag and the amb_5 peptides have more than two sites that can coordinate the Ni(II) and these could displace one or more of the NTA binding sites during the formation of the complex.

3.7 Competition of amb_5 for forming Ni(II) or Zn(II) complexes

The four amb_5 species **H**, **I**, **J**, and **N** which exhibited the highest selectivity for forming amb_5+Ni(II)+NTA were chosen with species **A** and **O**, as examples of the 2His-2Cys and 4His binding motifs, with the His-tag **P** to study how they compared for forming complexes of amb_5+M(II)+NTA from solutions that contained Zn(II), Ni(II) and NTA at pH 7.0. The relative formation of the Ni(II) complexes are higher than those of the Zn(II) complexes for all amb_5 species (Fig 6b), apart from **O** which is inconclusive due to its large error bar. The species **A**, **H**, and **N** all showed about the same percent formation of either complex with **I**, **J**, and **P** exhibiting the highest formation of the Ni(II) complex. The results show the percent formation of amb_5+Ni(II)+NTA by amb_5 **I** and **J** are the closest to the His-tag **P** but they also show a distinct selectivity for forming Ni(II) over Zn(II) complexes. This Ni(II) selectivity of **I** and **J** should be beneficial for recombinant protein purification because Zn(II) is widely distributed in the bacterial host cells and the tag remaining metal free during expression is necessary for the Ni-NTA-based IMAC purification.

3.8 The collision-induced dissociation of the $[amb_{5J}$+Ni(II)+NTA$]^-$ complexes

The amb_{5J}+Ni(II)+NTA complexes of **J** were observed with the charges of 2+, 1- and 2- and to investigate how relevant their structures were to the complex formed in an IMAC column, collision-induced dissociation of these complexes were conducted. The 2+ complex primarily dissociated into the $[amb_{5J}+Ni(II)]^{2+}$ complex by the loss of neutral NTA. The 1– complex $[amb_{5J}+Ni(II)+NTA]^-$ dissociated into the $[amb_{5J}-3H+Ni(II)]^-$ or $[NTA-3H+Ni(II)]^-$ complexes (Fig 7a), where by relating their relative abundances to the branching ratio for these competing reactions indicates $[amb_{5J}-3H]^{3-}$ has the higher Ni(II) formation constant than $[NTA-3H]^{3-}$. However, the 2– complex $[amb_{5J}+Ni(II)+NTA]^{2-}$ primarily

dissociated into $[NTA\text{-}3H+Ni(II)]^-$ and $[amb_{5J}\text{-}H]^-$ (Fig 7b) with only trace amounts of $[amb_{5J}\text{-}3H+Ni(II)]^-$ and $[NTA\text{-}H]^-$, indicating the Coulomb repulsion of the two negative charges of the complex influenced the branching ratio. These dissociation patterns could be useful for comparing the relative stability of the different amb_5 **A** to **R** for forming these complexes, and these studies are underway and will be presented in a future paper. Overall the dissociation of the $[amb_{5J}+Ni(II)+NTA]^-$ complexes shows they are realistic mimics for the complex inside an IMAC column.

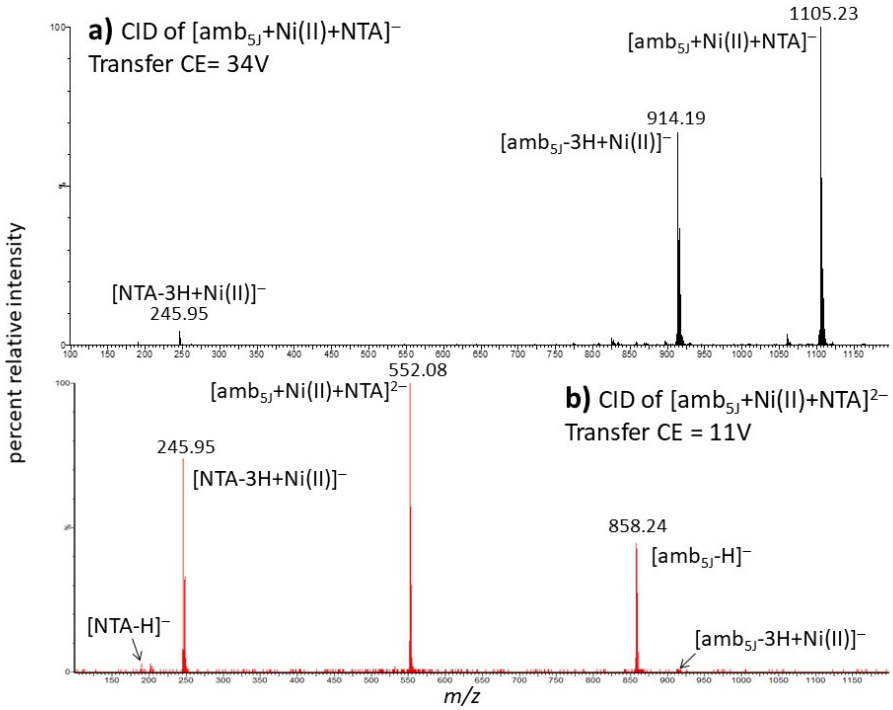

Figure 7. a) The collision-induced dissociation of $[amb_{5J}+Ni(II)+NTA]^-$ using a transfer collision energy of 34 V produced the products of $[amb_{5J}\text{-}3H+Ni(II)]^-$ and $[NTA\text{-}3H+Ni(II)]^-$ **b)** The collision-induced dissociation of $[amb_{5J}+Ni(II)+NTA]^{2-}$ using a transfer collision energy of 11 V produced the products of $[NTA\text{-}3H+Ni(II)]^-$, $[amb_{5J}\text{-}H]^-$, $[NTA\text{-}H]^-$ and $[amb_{5J}\text{-}3H+Ni(II)]^-$.

4. Conclusions

Here we have shown the results of our ESI-IM-MS and DFT study for comparing a series of amb_5 heptapeptides, with the general structure acetyl-Aa_1-Aa_2-Gly_3-Pro_4-Tyr_5-Aa_6-Aa_7, for forming complexes of amb_5+M(II) and amb_5+M(II)+NTA, where M = Co, Zn, and Ni. The results showed the amb_5 with 2 Cys in their primary structure (acetyl-Aa_1-Cys_2-Gly_3-Pro_4-Tyr_5-Aa_6-Cys_7) exhibited a preference for forming Zn(II) complexes, while those with 2 or 3 Asp in the structure (acetyl-Asp_1-Asp_2-Gly_3-Pro_4-

Tyr_5-His_6-Aa_7, where Aa_7 = Cys or Asp) exhibited a preference for forming Ni(II) complexes. These latter amb_5 species also showed the highest selectivity for forming the amb_5+Ni(II)+NTA complexes which suggests that they may be suitable as alternative tags for recombinant protein purification using the IMAC technique. Future work will compare the stability of these amb_5+M(II)+NTA complexes by comparing the energy-resolved CID dissociation of the complex and formation of products. Experiments are also underway for testing whether the new amb_5 tags can be used in the expression and purification of *β*-lactamase and whether our ESI-IM-MS techniques can be used to study the influence of the His- or amb_5-tag on the thermal stability and activity of the *β*-lactamase protein.

Acknowledgements

This material is based upon work supported by the National Science Foundation under 1764436, NSF instrument support (MRI-0821247), Welch Foundation (T-0014), and computing resources from the Department of Energy (TX-W-20090427-0004-50) and L3 Communications. We thank the Bower's group of University of California - Santa Barbara for sharing the Sigma program.

References

1. Amarasinghe, C.; Jin, J.-P., The Use of Affinity Tags to Overcome Obstacles in Recombinant Protein Expression and Purification. *Protein Pept. Lett.* **2015,** *22* (10), 885-892.

2. Bornhorst, J. A.; Falke, J. J., Purification of proteins using polyhistidine affinity tags. *Methods in enzymology* **2000,** *326*, 245-254.

3. Spriestersbach, A.; Kubicek, J.; Schäfer, F.; Block, H.; Maertens, B., Chapter One - Purification of His-Tagged Proteins. In *Methods in Enzymology*, Lorsch, J. R., Ed. Academic Press: 2015; Vol. 559, pp 1-15.

4. Booth, W. T.; Schlachter, C. R.; Pote, S.; Ussin, N.; Mank, N. J.; Klapper, V.; Offermann, L. R.; Tang, C.; Hurlburt, B. K.; Chruszcz, M., Impact of an N-terminal Polyhistidine Tag on Protein Thermal Stability. *ACS Omega* **2018,** *3* (1), 760-768.

5. Khan, F.; Legler, P. M.; Mease, R. M.; Duncan, E. H.; Bergmann-Leitner, E. S.; Angov, E., Histidine affinity tags affect MSP142 structural stability and immunodominance in mice. *Biotechnol. J.* **2012,** *7* (1), 133-147.

6. Choi, D. W.; Sesham, R.; Kim, Y.; Angel, L. A., Analysis of methanobactin from Methylosinus trichosporium OB3b via ion mobility mass spectrometry. *Eur. J. Mass Spectrom.* **2012,** *18* (6), 509-520.

7. McCabe, J. W.; Vangala, R.; Angel, L. A., Binding Selectivity of Methanobactin from *Methylosinus trichosporium* OB3b for Copper(I), Silver(I), Zinc(II), Nickel(II), Cobalt(II), Manganese(II), Lead(II), and Iron(II). *J. Am. Soc. Mass Spectrom.* **2017,** *28*, 2588-2601.

8. Sesham, R.; Choi, D.; Balaji, A.; Cheruku, S.; Ravichetti, C.; Alshahrani, A. A.; Nasani, M.; Angel, L. A., The pH dependent Cu(II) and Zn(II) binding behavior of an analog methanobactin peptide. *European Journal of Mass Spectrometry* **2013,** *19* (6), 463-473.

9. Choi, D.; Alshahrani, A. A.; Vytla, Y.; Deeconda, M.; Serna, V. J.; Saenz, R. F.; Angel, L. A., Redox activity and multiple copper(I) coordination of 2His-2Cys oligopeptide. *Journal of Mass Spectrometry* **2015,** *50* (2), 316-325.

10. Vytla, Y.; Angel, L. A., Applying Ion Mobility-Mass Spectrometry Techniques for Explicitly Identifying the Products of Cu(II) Reactions of 2His-2Cys Motif Peptides. *Anal. Chem.* **2016,** *88* (22), 10925-10932.

11. Wagoner, S. M.; Deeconda, M.; Cumpian, K. L.; Ortiz, R.; Chinthala, S.; Angel, L. A., The multiple conformational charge states of zinc(II) coordination by 2His-2Cys oligopeptide investigated by ion mobility - mass spectrometry, density functional theory and theoretical collision cross sections. *J. Mass Spectrom.* **2016,** *51* (12), 1120-1129.

12. Yousef, E. N.; Sesham, R.; McCabe, J. W.; Vangala, R.; Angel, L. A., Ion mobility-mass spectrometry techniques for determining the structure and mechanisms of metal ion recognition and redox activity of metal binding oligopeptides. *J. Visualized Exp.* **2019,** (151), e60102.

13. Lin, Y.-F.; Yousef, E. N.; Torres, E.; Truong, L.; Zahnow, J. M.; Donald, C. B.; Qin, Y.; Angel, L. A., Weak acid-base interactions of histidine and cysteine affect the charge states, tertiary structure, and Zn(II)-binding of heptapeptides. *J. Am. Soc. Mass Spectrom.* **2019,** *30* (10), 2068-2081.

14. Ilesanmi, A. B.; Moore, T. C.; Angel, L. A., pH dependent chelation study of Zn(II) and Ni(II) by a series of hexapeptides using electrospray ionization - Ion mobility - Mass spectrometry. *Int. J. Mass Spectrom.* **2020,** *455*, 116369.

15. Yousef, E. N.; Angel, L. A., Comparison of the pH-dependent formation of His and Cys heptapeptide complexes of nickel(II), copper(II), and zinc(II) as determined by ion mobility-mass spectrometry. *J. Mass Spectrom.* **2020,** *55* (3), e4489.

16. Pringle, S. D.; Giles, K.; Wildgoose, J. L.; Williams, J. P.; Slade, S. E.; Thalassinos, K.; Bateman, R. H.; Bowers, M. T.; Scrivens, J. H., An investigation of the mobility separation of some peptide and protein ions using a new hybrid quadrupole/travelling wave IMS/oa-ToF instrument. *International Journal of Mass Spectrometry* **2007,** *261* (1), 1-12.

17. Becke, A. D., A new mixing of Hartree-Fock and local-density-functional theories. *J. Chem. Phys.* **1993,** *98* (2), 1372-7.

18. Lee, C.; Yang, W.; Parr, R. G., Development of the Colle-Salvetti correlation-energy formula into a functional of the electron density. *Phys. Rev. B: Condens. Matter* **1988,** *37* (2), 785-9.

19. Zhao, Y.; Truhlar, D. G., The M06 suite of density functionals for main group thermochemistry, thermochemical kinetics, noncovalent interactions, excited states, and transition elements: two new functionals and systematic testing of four M06-class functionals and 12 other functionals. *Theor. Chem. Acc.* **2008,** *120* (1-3), 215-241.

20. Zhao, Y.; Truhlar, D. G., The M06 suite of density functionals for main group thermochemistry, thermochemical kinetics, noncovalent interactions, excited states, and transition elements: two new functionals and systematic testing of four M06-class functionals and 12 other functionals. [Erratum to document cited in CA149:183977]. *Theor. Chem. Acc.* **2008,** *119* (5-6), 525.

21. Frisch, M. J.; Trucks, G. W.; Schlegel, H. B.; Scuseria, G. E.; Robb, M. A.; Cheeseman, J. R.; Scalmani, G.; Barone, V.; Mennucci, B.; Petersson, G. A.; Nakatsuji, H.; Caricato, M.; Li, X.; Hratchian, H. P.; Izmaylov, A. F.; Bloino, J.; Zheng, G.; Sonnenberg, J. L.; Hada, M.; Ehara, M.; Toyota, K.; Fukuda, R.; Hasegawa, J.; Ishida, M.; Nakajima, T.; Honda, Y.; Kitao, O.; Nakai, H.; Vreven, T.; Montgomery, J., J. A.; Peralta, J. E.; Ogliaro, F.; Bearpark, M.; Heyd, J. J.; Brothers, E.; Kudin, K. N.; Staroverov, V. N.; Kobayashi, R.; Normand, J.; Raghavachari, K.; Rendell, A.; Burant, J. C.; Iyengar, S. S.; Tomasi, J.; Cossi, M.; Rega, N.; Millam, J. M.; Klene, M.; Knox, J. E.; Cross, J. B.; Bakken, V.; Adamo, C.; Jaramillo, J.; Gomperts, R.; Stratmann, R. E.; Yazyev, O.; Austin, A. J.; Cammi, R.; Pomelli, C.; Ochterski, J. W.; Martin, R. L.; Morokuma, K.; Zakrzewski, V. G.; Voth, G. A.; Salvador, P.; Dannenberg, J. J.; Dapprich, S.; Daniels, A. D.; Farkas, Ö.; Foresman, J. B.; Ortiz, J. V.; Cioslowski, J.; Fox, D. J. *Gaussian 09, Revision C.01*, Gaussian, Inc.: Wallingford CT, 2012.

22. Wachters, A. J. H., Gaussian basis set for molecular wavefunctions containing third-row atoms. *J. Chem. Phys.* **1970,** *52* (3), 1033-6.

23. Buchmann, W.; Spezia, R.; Tournois, G.; Cartailler, T.; Tortajada, J., Structures and fragmentations of cobalt(II)-cysteine complexes in the gas phase. *J. Mass Spectrom.* **2007,** *42* (4), 517-526.

24. Spezia, R.; Tournois, G.; Cartailler, T.; Tortajada, J.; Jeanvoine, Y., Co2+ binding cysteine and selenocysteine: a DFT study. *J. Phys. Chem. A* **2006,** *110* (31), 9727-9735.

25. Wyttenbach, T.; von Helden, G.; Batka, J. J., Jr.; Carlat, D.; Bowers, M. T., Effect of the long-range potential on ion mobility measurements. *J. Am. Soc. Mass Spectrom.* **1997,** *8* (3), 275-282.

26. Sovago, I.; Kallay, C.; Varnagy, K., Peptides as complexing agents: Factors influencing the structure and thermodynamic stability of peptide complexes. *Coord. Chem. Rev.* **2012,** *256* (19-20), 2225-2233.